

Catalysis Science & Technology

Accepted Manuscript



This is an *Accepted Manuscript*, which has been through the Royal Society of Chemistry peer review process and has been accepted for publication.

Accepted Manuscripts are published online shortly after acceptance, before technical editing, formatting and proof reading. Using this free service, authors can make their results available to the community, in citable form, before we publish the edited article. We will replace this *Accepted Manuscript* with the edited and formatted *Advance Article* as soon as it is available.

You can find more information about *Accepted Manuscripts* in the [Information for Authors](#).

Please note that technical editing may introduce minor changes to the text and/or graphics, which may alter content. The journal's standard [Terms & Conditions](#) and the [Ethical guidelines](#) still apply. In no event shall the Royal Society of Chemistry be held responsible for any errors or omissions in this *Accepted Manuscript* or any consequences arising from the use of any information it contains.

Conversion of Syngas-Derived C₂+ Mixed Oxygenates to C₃-C₅ Olefins over Zn_xZr_yO_z Mixed Oxides Catalysts

Colin Smith¹, Vanessa Lebarbier Dagle¹, Matthew Flake¹, Karthikeyan K. Ramasamy¹, Libor Kovarik², Mark Bowden², Thomas Onfroy³, and Robert A. Dagle^{1*}

¹Institute for Integrated Catalysis, Pacific Northwest National Laboratory, Richland, WA 99352, USA

²Environmental Molecular Sciences Laboratory, Pacific Northwest National Laboratory, Richland, WA 99352, USA

^{3a} Sorbonne University, UPMC Univ Paris 06, UMR 7197, Laboratoire de Réactivité de Surface, Paris, 75005, France

^{3b} CNRS, UMR 7197, Laboratoire de Réactivité de Surface, Paris, 75005, France

Submitted to *Catalysis Science & Technology*

Pacific Northwest National Laboratory

August, 2015

*Corresponding author: Robert.Dagle@pnnl.gov

Abstract

In this study we report on a $Zn_xZr_yO_z$ mixed oxide type catalyst capable of converting a syngas-derived C_2+ mixed oxygenate feedstock to isobutene-rich olefins. Aqueous model feed comprising of ethanol, acetaldehyde, acetic acid, ethyl acetate, methanol, and propanol was used as representative liquid product derived from a Rh-based mixed oxygenate synthesis catalyst. Greater than 50% carbon yield to C_3 - C_5 mixed olefins was demonstrated when operating at 400-450°C and 1 atm. In order to rationalize formation of the products observed feed components were individually evaluated. Major constituents of the feed mixture (ethanol, acetaldehyde, acetic acid, and ethyl acetate) were found to produce isobutene-rich olefins. C-C coupling was also demonstrated for propanol feedstock - a minor constituent of the mixed oxygenate feed - producing branched C_6 olefins, revealing scalability to alcohols higher than ethanol following an analogous reaction pathway. Using ethanol and propanol feed mixtures, cross-coupling reactions produced mixtures of C_4 , C_5 , and C_6 branched olefins. The presence of H_2 in the feed was found to facilitate hydrogenation of the ketone intermediates, thus producing straight chain olefins as byproducts. While activity loss from coking is observed complete catalyst regeneration is achieved by employing mild oxidation. For conversion of the mixed oxygenate feed a Zr/Zn ratio of 2.5 and a reaction temperature of 450°C provides the best balance of stability, activity, and selectivity. X-ray diffraction and scanning transmission electron microscopy analysis reveals the presence of primarily cubic phase ZrO_2 and a minor amount of the monoclinic phase, with ZnO being highly dispersed in the lattice. The presence of ZnO appears to stabilize the cubic phase resulting in less monoclinic phase as the ZnO concentration increases. Infrared spectroscopy shows the mixed oxide acid sites are characterized as primarily Lewis type acidity. The direct relationship between isobutene production and the ratio of basic/acidic sites was

demonstrated. An optimized balance of active sites for isobutene production from acetone was obtained with a basic/acidic site ratio of ~ 2 . This technology for the conversion of aqueous mixtures of C_2+ mixed oxygenates provides significant advantages over other presently studied catalysts in that its unique properties permit the utilization of a variety of feeds in a consistently selective manner.

Keywords: biomass, catalyst, mixed oxides, ethanol, acetic acid, propene, isobutene, hydrogen, oxygenates, syngas

1. Introduction

Production of liquid hydrocarbons from biomass is seen by many as a promising renewable source of transportation fuels¹⁻³ and chemicals.^{4,5} Currently, political drivers are in place for reducing the production of greenhouse gases and in fostering energy independence. Upgrading of ethanol to fuels and chemicals have been the subject of much attention because bioethanol is an important renewable feedstock as it currently accounts for 90% of the global biofuel production.⁶ However, other oxygenates can be produced from various bioprocesses as well. For example, gasification of biomass produces a syngas that can be used to produce a variety of fuels and chemicals.⁷ Recently, much work has been done developing catalysts for the production of higher alcohols and oxygenates from biomass-derived syngas.^{8,9} Fermentation products can also include acetates and higher alcohols in addition to ethanol. Additionally, product streams derived from direct liquefaction processes such as fast pyrolysis and hydrothermal liquefaction can include aqueous mixtures including alcohols, acids, aldehydes, and ketones, which often are present in small quantities.^{7,10} Despite significant research in the production of hydrocarbons from biomass, most of these processes still suffer from making an abundance of light oxygenates, often within complex mixtures. Efficient conversion of these light oxygenates to fuels or high value chemicals and with minimal separations is highly desirable.^{3,11-13}

$Zn_xZr_yO_z$ mixed oxide type catalysts with balanced acid-base sites were previously shown to be effective for converting ethanol to acetone, and subsequently acetone to isobutene, in a single-step process.¹⁴⁻¹⁶ Isobutene stoichiometric yields of approximately 83%, with 100% ethanol conversion were reported.¹⁵ In this study, we examine the effectiveness of a $Zn_xZr_yO_z$ mixed oxide catalyst¹⁶ for the conversion of a Rh-derived mixed oxygenate feedstock comprising of an

aqueous mixture of ethanol, acetaldehyde, acetic acid, and ethyl acetate, methanol, and propanol to isobutene-rich olefins. We assess performance under industrially relevant feed concentrations and gas-hour-space-velocities (GHSV), and explore the potential for generic C-C coupling and O₂ removal capability in the efficient conversion for a variety of small oxygenates such as alcohols, aldehydes, acids, and ketones to higher-order alkenes. Thus exploring feasibility for integration of this mixed oxides conversion technology with existing front-end conversion technologies that produce biological or thermochemical derived light oxygenates, and upgrading them to isobutene-rich olefins. Isobutene can be oligomerized over solid acid catalysts to form condensable alkenes targeted for gasoline, jet, and/or diesel fuel synthesis application.¹⁷ Isobutene is also an industrially relevant chemical that is widely used and can also be used as a fuel additive.¹⁸ New techniques for the synthesis of isobutene are presently relevant as isobutene is obtained primarily via catalytic steam cracking of fossil feedstocks making a carbon neutral technique highly desirable.¹⁹ The components within the mixed oxygenated feedstock were individually evaluated thus exploring the potential for feedstock flexibility of the mixed oxides catalyst. To understand the relationship between the catalytic performance and the catalyst properties, a series of Zn_xZr_yO_z mixed oxides with varied Zr/Zn ratios were characterized using combined X-ray diffraction (XRD), scanning transmission electron microscopy (STEM), and infrared spectroscopy (IR) techniques.

2. Experimental Details

2.1 Catalyst Preparation

Mixed oxide catalysts were synthesized via wet impregnation of a Zn(NO₃)₂·6H₂O solution on Zr(OH)₄ as described elsewhere.^{16, 20} The Zr(OH)₄ was initially dried overnight at 105°C to

remove any excess water on the surface before impregnation. After impregnation, the catalysts were dried overnight at room temperature and then for 4 hours at 105°C prior to calcination. The catalysts then were calcined via a 3°C/min ramp to 400°C for 2 hours, followed by a 5°C/min ramp to the final calcination temperature of 550°C for 3 hours.

2.2 Catalyst Characterization

STEM measurements were conducted with a FEI Titan 80-300 operated at 300 kV. The FEI Titan is equipped with CEOS GmbH double-hexapole aberration corrector for the probe-forming lens, which allows imaging with ~0.1 nm resolution in STEM mode. The STEM images were acquired on a high angle annular dark field with an inner collection angle of 52 mrad. In general, the TEM sample preparation involved mounting powder samples on copper grids covered with lacey carbon support films and then immediately loading them into the TEM airlock to minimize exposure to atmospheric O₂.

XRD spectra were recorded using a Philips X'pert MPD (Model PW3040/00) diffractometer with a copper anode ($K\alpha_1 = 0.15405$ nm) and a scanning rate of 0.002° per second between $2\theta = 10^\circ$ to 80° . The diffraction patterns were analyzed using Jade 5 (Materials Data Inc., Livermore, CA) and the Powder Diffraction File database (International Center for Diffraction Data, Newtown Square, PA). Quantitative XRD analysis was performed by full-pattern (Rietveld) refinement²¹ using the TOPAS program (v 4.2, Bruker AXS). In this procedure, patterns were calculated from crystal structures obtained from the Inorganic Crystal Structure Database (Fachinformationszentrum Karlsruhe, Germany), and peak shapes were modeled using the fundamental parameters approach.

N₂ adsorption was measured at 77 K with an automatic adsorptiometer (Micromeritics ASAP 2000). Samples were pretreated at 150°C for 12 hours under vacuum. The surface areas were

determined from adsorption values for five relative pressures (P/P_0) ranging from 0.05 to 0.2 using the Brunauer-Emmett-Teller (BET) surface method. The pore volumes were determined from the total amount of N_2 adsorbed between $P/P_0 = 0.05$ and $P/P_0 = 0.98$.

CO_2 chemisorption experiments were conducted with a home-made system consisting of a micro-reactor equipped with a VICI valve (Valco) and connected to a mass spectrometer (Pfeiffer, OMNISTAR Model GSD 301) for online analysis. For each experiment, 50 mg of catalyst was loaded between two layers of quartz wool using a quartz tube reactor with a 4 mm inner diameter. A thermocouple was placed in the middle of the catalyst bed, and the temperature was followed online using Daqview. Before each experiment, the catalyst was treated *in situ* under N_2 at $450^\circ C$ for 8 hours. Then, the temperature was decreased to $30^\circ C$, and 20 pulses of CO_2 (60% CO_2 in helium) were first introduced to measure the number of chemisorbed + physisorbed CO_2 . After that, the system was flushed for 30 minutes under helium and 20 more pulses of CO_2 were introduced to measure the number of physisorbed CO_2 .

Infrared spectra were recorded with a Nicolet 5700 Fourier transform-infrared (FT-IR) spectrometer equipped with a deuterated triglycine sulfate (DTGS) detector (resolution: 4 cm^{-1} , 128 scans). Prior to analysis the samples were pressed into pellets (ca. 20 mg for a 2 cm^2 pellet), activated under vacuum at $450^\circ C$ for 2 hours, and then cooled to $150^\circ C$. After activation, pyridine was introduced at $150^\circ C$ ($P_{\text{equilibrium}} = 133\text{ Pa}$), and the spectra was recorded following desorption from 150 to $350^\circ C$. The number of Brønsted acid sites titrated by pyridine was calculated using integrated molar absorption coefficient value of $\epsilon = 1.67\text{ cm}\cdot\mu\text{mol}^{-1}$ for ν_{19b} vibration of protonated pyridine at ca. 1548 cm^{-1} .²² The number of Lewis acid sites also titrated by pyridine was calculated using integrated molar absorption coefficient value of $\epsilon = 2.22\text{ cm}\cdot\mu\text{mol}^{-1}$ for ν_{19b} vibration of coordinated pyridine at ca. 1455 cm^{-1} .²²

2.3 Catalytic Activity

Catalytic activity tests for the conversion of aqueous oxygenated feeds were conducted in a 6.35mm outer diameter (inner diameter = 4.57 mm) fixed-bed packed bed reactor loaded with 1.0 g of $Zn_xZr_yO_x$ mixed oxide catalyst. A K-type thermocouple was placed in the reactor for measurement of the catalyst bed temperature. To minimize temperature gradients, an electrical resistance heating block was installed for temperature control. Prior to testing, catalysts were first activated *in situ* at 450°C for 8 hours under N_2 . Then N_2 and/or H_2 were introduced into the system using a Brooks mass flow controller (5850E series). Aqueous oxygenated feeds were fed into the system and converted to gas phase using a vaporizer consisting of 6.6 mm inner diameter steel tubing filled with quartz beads and ISCO syringe pump. The effects of conversion and selectivity were measured over a range of temperatures (375 to 450°C), pressures (1 to 20 atm), and GHSVs as noted. N_2 was typically used as the carrier gas. A knockout pot placed directly downstream of the reaction zone was used to collect liquid product. Gaseous effluent was analyzed online using an Inficon micro GC (Model 3000A) equipped with MS-5A, Plot U, alumina, and OV-1 columns and a thermal conductivity detector. Liquid samples collected from the knockout pot were analyzed separately *ex situ* using liquid chromatography. Catalyst regeneration was performed *in situ* at 550°C under flowing 5% O_2/He for 8 hours. This mild oxidative treatment is included to decoke the catalyst surface. During this treatment, CO_2 typically was observed and was considered to be indicative of carbon burn-off. Upon completion, the catalyst was then cooled to the desired reactor operating temperature under N_2 .

3. Results and Discussion

3.1 Ethanol Conversion over $\text{Zn}_1\text{Zr}_{10}\text{O}_2$

Sun and Liu recently reported the conversion of ethanol to isobutene over $\text{Zn}_x\text{Zr}_y\text{O}_z$ mixed oxide type catalysts.^{14, 15} Starting from ethanol, a complex sequence of reactions was shown to produce isobutene in a single catalytic step. These reactions include a variety of steps such as dehydrogenation, dehydration, condensation, and decomposition that require a balance of acid and base sites working in tandem.²³⁻²⁵ The general reaction network can be seen in Figure 1. Ethanol is first dehydrogenated to acetaldehyde and then oxidized to acetic acid, which undergoes ketonization to form acetone. All of these first steps are believed to occur quite readily.^{12, 24} Acetone conversion to isobutene follows a more complex but well studied pathway. Historically, zeolites such as HZSM-5 were thought to catalyze acetone condensation to diacetone alcohol and the subsequent dehydration to mesityl oxide over acidic Bronsted sites and this pathway was demonstrated with an NMR study²⁶, though FTIR investigations suggested Lewis sites also played an active role.²⁷ More recently several oxides such as Al_2O_3 , CeO_2 , ZrO_2 , and TiO_2 were shown to follow a similar route in FTIR studies.^{25, 28} These ethanol to isobutene pathways are supported by the results of this study as, with the exception of diacetone alcohol and mesityl oxide which are expected to be short lived in our reaction conditions^{29, 30}, all suggested intermediates have been observed in the product slate. Conversion of the acetone intermediate is the rate-limiting step, and acetone is sometimes present in the product. This is illustrated in Figure 2 where the increasing ethanol feed concentration corresponds to an increase in acetone selectivity and decrease in isobutene selectivity. Propene also is observed as a minor byproduct. In the presence of hydrogen, acetone can also undergo hydrogenation to form 2-propanol that subsequently can be dehydrated to propene. When ethanol is used as the feed, H_2

is formed *in situ* from the dehydrogenation of ethanol to acetaldehyde, thus facilitating the acetone hydrogenation and subsequent propene formation. In addition, the acidic properties of the catalyst do provide some dehydration activity, as evidenced by the production of propene and also mesityl oxide, which we speculate to be an intermediate¹⁵ as illustrated in Figure 2, although we have not detected its presence in this work. While some dehydration activity is necessary to convert diacetone alcohol to mesityl oxide, too much encourages an undesirable competing reaction in the direct dehydration of alcohols such as the formation of ethylene from ethanol. Finally, a small amount of methane also is formed from acetone decomposition, which is suggested to occur over similar sites used for the condensation reaction between acetone.²⁵ Thus, with ethanol feedstock, major products include isobutene, CO₂, and unreacted acetone and minor products include methane, ethene, and propene. It also should be noted that aqueous streams containing ethanol can be converted to these products without prior separation of ethanol and water.

3.2 Syngas-Derived Mixed Oxygenate Feedstock

The use of biomass-derived syngas to produce higher alcohols such as ethanol has been the subject of much research.^{7, 9} Supported Rh-based catalysts have the highest activity and selectivity for the formation of ethanol and other C₂+ oxygenates because of their ability to catalyze both CO dissociation and CO insertion.⁹ Using combined experimental and theoretical approaches, we previously developed a Rh-based catalyst with the goal of achieving high selectivity to C₂+ oxygenates through optimum choice of metal loading, promoters, and support.³¹⁻³⁴ This effort culminated in the design of a RhMnIr-based catalyst supported on carbon. This catalyst provided a selectivity to C₂+ oxygenates of 73% when operating under syngas with a H₂/CO = 1.3 molar ratio (containing 3 mol% CO₂), at 80 atm, 260°C, and a GHSV

of 13,000 L/kg_{cat}/hr.³² A representative composition for the produced aqueous mixed oxygenates is shown in Table 1. Primary products include ethanol, acetaldehyde, ethyl acetate, and acetic acid. Minor constituents include methanol and propanol. This composite mixture was vaporized and used as the feed for the C₃-C₅ olefins generation over mixed oxide catalyst.

The effect of temperature on catalyst performance for the liquid feed composite (Table 1) over Zn₁Zr₁₀O₂ is shown in Figure 3. With increasing temperature for a given residence time, a decrease in acetone selectivity coincides with an increase in isobutene and CO₂ selectivity, indicating that higher temperature facilitates acetone conversion towards the desired C₄ olefin product. However, in addition to an increased production of isobutene, it is apparent that increasing temperature also favors acetone decomposition, which results in increasing methane formation. While isobutene production appears to increase linearly with rising temperature, methane formation becomes significantly more pronounced by 450°C. This suggests that a balance needs to be found between facilitating acetone conversion to isobutene while minimizing the decomposition reaction to methane. Interestingly, among the olefins produced, ethene production remains relatively flat with increasing temperature; however, production of both propene and pentene increases. This implies that the rate for direct dehydration from ethanol to ethene is not greatly affected by temperature. On the contrary, the alternative reaction path that includes hydrogenation and carbon coupling are more prevalent at higher temperatures.

Duration studies over a period of 100 hours were performed over Zn₁Zr₁₀O₂ using the mixed oxygenate feed mixture to examine the catalyst's stability and ability to be regenerated. As shown in Figure 4, a gradual deactivation was observed during the first 70 hours with acetone selectivity doubling from approximately 25 to 50% while isobutene production decreased from 40 to 20%. The catalyst was regenerated *in situ* under mild oxidation conditions (550°C under

flowing 5% O₂/He for 8 hours), and then activity measurements were resumed. The catalyst was fully regenerated as evidenced by the restoration of isobutene selectivity to approximately 40%. This indicates that the bulk of deactivation resulted from the formation of coking side products that blocked the active sites for acetone conversion. It should be noted that selectivities for products such as methane, ethane, propene, methane, and CO₂ did not change significantly during the entire 100 hour duration.

3.3 Single Feed Component Evaluations

In order to understand the contribution to catalyst performance for each of the components within the mixed oxygenate feed mixture, constituents were separately evaluated in the presence of water. Ethanol, acetic acid, acetaldehyde, ethyl acetate, 1-propanol, and methanol were individually evaluated for conversion over the mixed oxides catalyst. Catalyst performance results are shown in Table 2. Ethanol, acetic acid, and acetaldehyde all result in similar product distributions, which is not unexpected as acetic acid and acetaldehyde are intermediates within the reaction network from ethanol as illustrated in Figure 1. Ethyl acetate in the presence of water undergoes hydrolysis to form ethanol and acetic acid, both of which then proceed along the same reaction pathway thus rendering a similar product distribution with isobutene and CO₂ being the primary products. One difference between the product slates is that no propene is formed when acetic acid is used. In the case of ethanol, H₂ is produced *in situ* as a result of ethanol dehydrogenation, thus facilitating the hydrogenation of acetone to isopropanol, which is then dehydrated to propene. With acetic acid, no dehydrogenation occurs, thus the necessary H₂ required for hydrogenation of acetone to occur is not available. With acetaldehyde, we believe that a small amount of decomposition of acetaldehyde occurs³⁵, thus producing the necessary H₂ to explain the small amount of propene observed. It should be noted that H₂ was

observed in the gas effluent for acetaldehyde and not in the case of acetic acid. When methanol is used as feed, CO₂ and H₂ are produced as a result of the steam reforming reaction.

Propanol makes a completely different product slate that includes C₂-C₆ olefins, ketones (acetone, methyl ethyl ketone, and 3-propanone), CO₂, and a small amount of saturated light hydrocarbons. We believe the C₆ olefins are produced in a pathway analogous to that of ethanol, and the reaction network is outlined in Figure 5(a). Propanoic acid is produced from propanol in a similar manner as acetic acid is produced from ethanol (as shown in Figure 1); thus, this portion of the sequence is not explicitly shown. Ketonization of propanoic acid produces 3-pentanone, which then undergoes a sequence of reactions that includes condensation and decomposition resulting in the formation of the branched C₆ olefins 2-ethyl-1-butene and 2-ethyl-2-butene, and methyl ethyl ketone (MEK). The C₄ and C₅ olefins also are formed and are believed to be products derived from MEK in reaction chemistry similar to that discussed below. The complete conversion of propanol coupled with C₆ olefin production suggests that the catalyst is functional for the conversion of higher alcohols (C₂+) in a reaction scheme analogous to ethanol. However, the comparatively high concentration of leftover ketone intermediates indicates that this activity is reduced, possibly because of steric effects.

3.4 Hydrogen and Pressure Effects

We also evaluated the consequences of the presence of H₂ in the feed. Acetic acid was used as feedstock to exclude the production of H₂ that would be produced from ethanol dehydrogenation if ethanol was used. As discussed above, no H₂ is formed *in situ* with acetic acid. The effect of varying the H₂ concentration in the acetic acid feed is shown in Table 3. Increasing the concentration of H₂ in the carrier gas corresponds to increasing propene formation facilitated by acetone hydrogenation. Without H₂ addition, no propene was produced. As a

practical consideration, this suggests that product formation can be tuned between isobutene and propene by adding or removing H₂ from the system.

We also explored the effect of operating pressure on ethanol conversion, and the results are shown in Table 4. While the product distribution remains fairly consistent in the pressure ranges studied, the propene selectivity increased from 5.4 to 10.9% as the system pressure was increased from 1 to 20 atm. Thus, there is an enhancement in acetone hydrogenation at higher pressures. However, the effect is not as significant as with direct H₂ addition and does not seem to significantly discourage the primary reaction pathway.

3.5 Ethanol-Propanol Binary Feed Mixtures

The effect of adding propanol to an ethanol feed was investigated over Zn₁Zr₁₀O₂. As shown in Table 5, increasing the propanol feed concentration corresponds to increasing C₅ olefin product selectivity and decreasing C₄ olefin product selectivity. This coupling of ethanol and propanol explains the formation of C₅ from the mixed oxygenate feed. The predominant reaction pathway believed to occur for the ethanol-propanol binary feed constituency is shown in Figure 5(b). Acetic acid and propionic acid are formed from their respective parent alcohols ethanol and propanol, respectively, as illustrated in Figure 1 for acetic acid. In addition to the 3-pentanone and acetone formed from independent reactions of propanoic and acetic acid as discussed earlier, cross condensation between the two acids can result in the production of asymmetric MEK. MEK then can undergo similar condensation/decomposition chemistry with either itself or other ketones such as acetone, resulting in branched C₅ olefins (specifically, 2-methyl-2-butene and 2-methyl-1-butene are formed approximately in equal amounts). Figure 5(a) illustrates this reaction pathway for acetone and MEK to produce acetaldehyde and a C₅ olefin. However, because of the asymmetric nature of MEK, acetone and propanaldehyde also are

potential byproducts of C₅ formation in the presence of MEK and acetone. In addition, straight-chained C₄ and C₅ products also can be formed via hydrogenation of the ketone intermediates to iso-alcohols and the subsequent dehydration of these alcohols to create olefins in chemistry analogous to propene formation.

Comparing branched and straight product formation demonstrates the relative favorability of the coupling reactions over the hydrogenation/dehydration pathway (Table 5). While the 10 wt% propanol and 10 wt% ethanol initially appear to favor straight C₄ formation, this is largely due to the abundance of MEK formed at the expense of acetone production, which is the precursor to isobutene. Isobutene formed through intermediate acetone as shown in Figure 1 is the primary species identified in the C₄ product slate.

Furthermore, the effect of temperature for a 15 wt% ethanol and 5 wt% propanol feed also is shown in Table 5. At 375°C, a significant amount of 3-pentanone and MEK are formed through the ketonization reactions shown in Figure 5. As the temperature is increased, these ketones are converted to additional olefins. It appears that these reactions do not proceed as rapidly as in the case of ethanol-derived acetone from conversion to olefin. Nonetheless, when propanol is added to ethanol, C₄ and C₅ olefins can be produced given adequate residence time or temperature.

3.6 Acid-Base Tuning for Performance Optimization

The relationship between the acidic and basic properties of the catalyst, and catalyst performance for conversion of the mixed oxygenate feed, was explored by varying the Zr/Zn composition. The Zn_xZr_yO_z catalyst is designed to maximize the inclusion of mostly basic properties of ZnO and the largely acidic properties of the ZrO₂ to achieve an ideal mix of acidic and basic sites capable of carrying out the variety of steps involved in upgrading oxygenates to

isobutene. Using the mixed oxygenated feed mixture (Table 1), the Zr/Zn ratio was varied, and the results are shown in Table 6. In all cases, complete carbon conversion was achieved. The lowest and highest Zr/Zn ratios have the largest acetone selectivities and lowest isobutene selectivities of the catalysts evaluated, reinforcing the notion that a balance is required to carry out the acetone condensation and coupling reactions necessary for isobutene production. An optimum Zr/Zn ratio of 2.5 to 5.0 was found to maximize isobutene selectivity. In addition, catalyst stability was compared for mixed oxides with Zr/Zn ratios of 2.5 and 10.0. As shown in Figure 6, the mixed oxide with higher zinc content (Zr/Zn = 2.5) was demonstrated to be more stable. As deactivation from coking largely occurs over acid sites, it follows that decreased number of total acid sites (see Table 7) provide a more stable catalyst.

We performed microstructure analysis of the $Zn_xZr_yO_z$ mixed oxides using a combination of TEM/STEM and energy dispersive spectroscopy techniques. Results from morphological and structural analysis, shown in Figure 7, revealed that the particles have rounded, but irregular, shapes and are mostly less than 20 nm in size. Based on high-resolution imaging and selected area diffraction, we found that the vast majority of the powder particles are structurally consistent with cubic ZrO_2 phase; only a very weak diffraction signal consistent with a hexagonal ZnO phase was identified in the agglomerated powder. The imaging and diffraction analysis was complemented by high angle annular dark field imaging and compositional analysis performed at multiple locations, as shown in Figure 7. The energy dispersive spectroscopy analysis shows Zn to be present across all ZrO_2 phase, and the amount of Zn varies with the highest enrichment detected at Zr/Zn ratio of ~ 4 . Therefore, it can be postulated that the Zn identified in this region is either incorporated in the structure of ZrO_2 or spread on the surface in

the form of clusters/rafts. The level of Zn associated with ZrO_2 is lower, however, than the nominal ratio of Zr/Zn of 2.5 because a fraction of Zn is lost in the ZnO phase.

To examine the effect of zinc concentration on the properties of the catalyst, quantitative XRD analyses were performed using the two Zr/Zn ratios of 2.5 and 10.0. In both catalysts, the dominant phase was found to be stabilized ZrO_2 . While tetragonal and cubic ZrO_2 crystals are difficult to differentiate, the lack of a characteristic tetragonal peak typically found at 43.4° suggests the stabilized ZrO_2 phase is cubic. Interestingly, more of the cubic phase was found in the lower ratio catalyst at 91% compared to 81% seen in the $\text{Zn}_1\text{Zr}_{10}\text{O}_2$. This was due to the much larger prevalence of the monoclinic phase in the 10/1 catalyst, making up 19% compared to 7%. In Figure 8, this is easily seen in the much larger shoulder at 27° . This is consistent with past literature exploring the relationship of mixed oxide systems wherein the cubic and tetragonal ZrO_2 phases are greatly stabilized by the presence of other metals in the lattice.^{36, 37} While 2% ZnO was observed in the $\text{Zn}_1\text{Zr}_{2.5}\text{O}_2$ catalyst, none with a ratio of 10 was detected, indicating the zinc was highly dispersed and incorporated in the lattice. The 2% ZnO found in the lower ratio suggests that an abundance of available zinc will result in a separate undesirable phase, which could explain why further decreasing the Zr/Zn ratio resulted in a rapid decrease in catalyst activity towards acetone to isobutylene conversion

To understand the relationship between the catalytic performance and the catalyst surface properties, the basic and acid sites have been quantified for the series of $\text{Zn}_x\text{Zr}_y\text{O}_z$ catalysts with different Zr/Zn ratios except for the Zr/Zn ratio corresponding to 15/1. First, we conducted CO_2 chemisorption experiments to determine the number of basic sites, and the results are presented in Table 7. It can be seen that the amount of CO_2 chemisorbed increases with the ZrO_2 content from 57 to 120 $\mu\text{moles/g}$. Note that the experiments have been repeated for several catalysts and

were found very reproducible (error within 1%). These results demonstrate that the amount of basic sites increases with the ZrO_2 content (i.e. increase of Zr/Zn ratio). The CO_2 TPD signals obtained after chemisorption are presented in Figure 9. One can see one major peak at $\sim 75^\circ\text{C}$ and a shoulder at $\sim 200^\circ\text{C}$ and no major difference is seen between all the TPD signals. These results suggest that these catalysts present similar basic sites strength.

The acid sites of the catalysts were identified and quantified by pyridine adsorption/desorption followed by IR spectroscopy. Figure 10 presents the IR spectra recorded between 1400 and 1700 cm^{-1} after pyridine adsorption at 150°C followed by a desorption at 150°C for 30 minutes. The bands observed at 1609, 1589, 1575, and 1450 cm^{-1} are attributed to the presence of pyridine coordinated to Zr^{4+} and/or Zn^{2+} and characteristic of Lewis acid sites.³⁸
³⁹ In addition, small bands characteristic of Brønsted acid sites also were detected at 1648 and 1551 cm^{-1} .¹⁴ We determined the number of Lewis and Brønsted acid sites from these spectra and the results are presented in Table 7. The results show that the number of Lewis acid sites is one order of magnitude higher than the number of Brønsted acid sites. Hence, these catalysts present mainly Lewis type acidity. Both the number of Brønsted acid sites and the number of Lewis acid sites determined after desorption at 150°C increase when the Zr/Zn ratio increases from 1/1 to 10/1. The results obtained after desorption at 350°C , also presented in Table 7 indicate that the total number of stronger Lewis acid sites is similar for the catalysts with Zr/Zn ratios of 1/1, 2.5/1, and 5/1, and inferior to the one obtained for the catalyst with a Zr/Zn ratio of 10/1. Note that bands characteristic of stronger Brønsted acid sites were not detected after desorption at 350°C except for the 10/1 ratio. The conversion of acetone to isobutene requires both basic and acid sites. We have thus shown in Figure 11 the evolution of isobutene production as well as the evolution of the ratio basic/acid sites number as a function of the Zr/Zn

ratio. Note that the acid sites number was determined from the spectra collected after desorption at 150°C and characteristic of all the acid sites (i.e. weaker, medium and stronger acid sites). Isobutene production increases when the Zr/Zn ratio increases from 1/1 to 2.5/1 and decreases with greater loading of ZrO₂. The same trend is observed when the ratio basic/acid sites number is reported as a function of the Zr/Zn ratio. This clearly demonstrates the existence of a direct relationship between isobutene production and the ratio of basic/acid sites. These results also show that an optimized balance of active sites for isobutene production from acetone is obtained for a ratio basic/acid sites number equal to ~2.

4. Conclusions

Following previous work in which the use of a mixed ZnO/ZrO₂ catalyst was found effective for the production of isobutene from ethanol, we demonstrate conversion of an aqueous oxygenated feed mixture, replicating the liquid products of an Rh-based syngas conversion catalyst, to isobutene-rich olefins. A mixed oxygenate feed comprising of ethanol, acetaldehyde, acetic acid, ethyl acetate, methanol, and propanol was found to produce C₃-C₅ olefins with > 50% carbon yield when operating at 400-450°C and 1 atm. Acetic acid and acetaldehyde proceed along the same reaction pathway as ethanol, thus generating a similar product slate. However, without the addition of H₂ propene is not produced, unlike with ethanol where H₂ is produced as a byproduct. Ethyl acetate undergoes hydrolysis to form acetic acid and ethanol that, in turn, proceeds along the same pathway. Methanol produced CO₂ and H₂ as a result of steam reforming. Propanol feed produced branched C₅ olefins from a 3-pentanone intermediate, thus proceeding along an analogous reaction pathway as isobutene produced from ethanol through acetone intermediate. In optimizing catalytic performance for conversion of the mixed oxygenate feed, we found that a Zr/Zn ratio of 2.5 and a reaction temperature of 450°C provided

the best balance of stability, activity, and selectivity. Over a period of 70 hours, $\text{Zn}_1\text{Zr}_{10}\text{O}_2$ catalyst selectivity towards isobutene decreased from approximately 40 to 20% because of coke formation; however, in situ mild oxidative regeneration restored the catalyst to its original activity. The ZnO/ZrO_2 system was demonstrated to be versatile in its upgrading and coupling activity, handling a variety of light oxygenates while consistently following a similar reaction pathway resulting in isobutene and other comparable branched olefins.

Combined XRD and TEM analysis revealed that the catalyst mostly consisted of cubic phase ZrO_2 and a minor amount of the monoclinic phase, with zinc being highly dispersed in the lattice. The presence of zinc appears to stabilize the cubic phase resulting in less monoclinic phase with increasing zinc concentration. Pyridine adsorption/desorption followed by IR spectroscopy showed the mixed oxide acid sites to be characterized by Lewis type acidity. A clear correlation between the ratio of basic/acid sites and isobutene production from the mixed oxygenate feed mixture was established, with optimum olefin selectivity requiring a basic/acid site ratio of ~ 2 .

Acknowledgements

This work was financially supported by the U.S. Department of Energy (DOE) Bioenergy Technologies Office and was performed at Pacific Northwest National Laboratory (PNNL). PNNL is a multi-program national laboratory operated for DOE by Battelle Memorial Institute. Advanced catalyst characterization use was granted by a user proposal at the William R. Wiley Environmental Molecular Sciences Laboratory, which is a national scientific user facility sponsored by DOE's Office of Biological and Environmental Research and located at PNNL. The authors would like to thank Theresa Lemmon and Marie Swita for analytical support of this project. Finally, the authors would like to thank Cary Counts of PNNL for help with technical editing of this manuscript.

Table Captions

Table 1. Mixed oxygenate feed concentration.

Table 2. Catalytic performance comparisons for single oxygenated feeds over $\text{Zn}_1\text{Zr}_{10}\text{O}_2$ ($T = 450^\circ\text{C}$, $P_T = 1 \text{ atm}$, $P_{\text{N}_2} = 0.50 \text{ atm}$, $\text{GHSV} = 5,000 \text{ h}^{-1}$).

Table 3. Effect of H_2 addition using 10 wt% acetic acid (balance H_2O) liquid feed over $\text{Zn}_1\text{Zr}_{10}\text{O}_2$ ($T = 450^\circ\text{C}$, $P_T = 1 \text{ atm}$, $P_{\text{N}_2+\text{H}_2} = 0.50 \text{ atm}$, $\text{GHSV} = 5,000 \text{ h}^{-1}$).

Table 4. Effect of operating pressure when using 20 wt% ethanol (balance H_2O) liquid feed over $\text{Zn}_1\text{Zr}_{10}\text{O}_2$ ($T = 450^\circ\text{C}$, $P_T = 1 \text{ atm}$, $P_{\text{N}_2} = 0.50 \text{ atm}$, $\text{GHSV} = 5,000 \text{ h}^{-1}$).

Table 5. Effect of propanol addition to ethanol feed over $\text{Zn}_1\text{Zr}_{10}\text{O}_2$ ($T = 450^\circ\text{C}$, $P_T = 1 \text{ atm}$, $P_{\text{N}_2} = 0.50 \text{ atm}$, $\text{GHSV} = 5,000 \text{ h}^{-1}$).

Table 6. Catalytic performance comparisons using a mixed oxygenate feed mixture (Table 1) over mixed oxide catalysts with varied acid and base properties ($T = 450^\circ\text{C}$, $P_T = 1 \text{ atm}$, $P_{\text{N}_2} = 0.50 \text{ atm}$, $\text{GHSV} = 3,800 \text{ h}^{-1}$).

Table 7. BET surface area, pore volume, pore diameter, acidity and basicity site quantification, and butene production as a function of Zr/Zn ratio.

Figure Captions

Figure 1. Reaction network for the conversion of ethanol to isobutene (and major side products).

Figure 2. Effect of varying ethanol feed concentration on product selectivity over $\text{Zn}_1\text{Zr}_{10}\text{O}_2$ ($T = 425^\circ\text{C}$, $P = 1 \text{ atm}$, $\text{GHSV} = 15,500 \text{ h}^{-1}$, $\text{S/C} = 5 \text{ mol}$; ethanol conversion = 100% for all data points).

Figure 3. Effect of temperature on product selectivity for the mixed oxygenate feed mixture (Table 1) over $\text{Zn}_1\text{Zr}_{10}\text{O}_2$ ($P_T = 1 \text{ atm}$, $P_{\text{N}_2} = 0.60 \text{ atm}$, $\text{GHSV} = 3,800 \text{ h}^{-1}$).

Figure 4. Stability and regeneration demonstration with the mixed oxygenate feed mixture (Table 1) over $\text{Zn}_1\text{Zr}_{10}\text{O}_2$. $T = 425^\circ\text{C}$, $P_T = 1 \text{ atm}$, $P_{\text{N}_2} = 0.60 \text{ atm}$, $\text{GHSV} = 3,800 \text{ h}^{-1}$. Decoking procedure performed via mild oxidative treatment after a time-on-stream of ~ 72 hours. Catalyst regeneration demonstrated as evidenced by selectivity recovery.

Figure 5. Reaction network for the conversion of (a) propanoic acid to form C_5 and C_6 olefins. Propanoic acid is formed from its parent alcohol propanol via dehydrogenation/oxidation as illustrated in Figure 1 and (b) propanoic acid and acetic acid mixtures to form C_4 and C_5 olefins. Propanoic and acetic acid are formed from their parent alcohol propanol and ethanol via dehydrogenation/oxidation as illustrated in Figure 1.

Figure 6. Stability comparison using the mixed oxygenate feed mixture (Table 1) over mixed oxide catalysts with varied acid and base properties. Catalysts: $\text{Zn}_1\text{Zr}_{10}\text{O}_2$ ($\text{Zr/Zn} = 10$) and $\text{Zn}_1\text{Zr}_{2.5}\text{O}_2$ ($\text{Zr/Zn} = 2.5$). $T = 425^\circ\text{C}$, $P_T = 1 \text{ atm}$, $P_{\text{N}_2} = 0.60 \text{ atm}$, $\text{GHSV} = 3,800 \text{ h}^{-1}$.

Figure 7. TEM (A) images and (B) EDX elemental mapping for the $\text{Zn}_1\text{Zr}_{2.5}\text{O}_2$ ($\text{Zr/Zn} = 2.5$) mixed oxide catalyst.

Figure 8. XRD patterns for the catalysts with Zr/Zn ratios equal to 2.5 and 10.

Figure 9. CO_2 TPD signal for the $\text{Zn}_x\text{Zr}_y\text{O}_z$ catalysts with Zr/Zn ration between 1 and 10.

Figure 10. Infrared spectra recorded after pyridine adsorption at 150°C followed by desorption at the same temperature for 30 minutes. Spectra normalized to 10 mg of catalyst and for a pellet of 2 cm^2 .

Figure 11. Relationship between butene production (activity data extracted from Table 6) and the ratio of basic to acidic sites as a function of the Zr/Zn ratio. The acid sites concentration was determined from the IR spectra collected after pyridine desorption at 150°C .

Table 1. Mixed oxygenate feed concentration.

Component	Wt%
Ethanol	17.2
Acetic Acid	9.8
Acetaldehyde	10.3
Ethyl Acetate	9.9
Methanol	1.1
1-Propanol	2.0
H ₂ O	49.7

Table 2. Catalytic performance comparisons for single oxygenated feeds over Zn₁Zr₁₀O₂ (T = 450°C, P_T = 1 atm, P_{N₂} = 0.50 atm, GHSV = 5,000 h⁻¹).

Feed (wt.%)	X _{carbon} (%)	Selectivity (mol C %)											Total
		CH ₄	CO ₂	Olefins					Alkanes	Ketones			
				C ₂	C ₃	C ₄	C ₅	C ₆	C ₂ -C ₅	Acetone	MEK	3-Pentanone	
20% ethanol	>99	6.8	32.2	1.7	5.4	42.4	0	0	0	11.1	0	0	100
10% acetic acid	>99	13.8	42	0	0	37.6	0	0	0	6.5	0	0	100
10% acetaldehyde	>99	11	36.4	0	3.2	38.8	0	0	0	10.6	0	0	100
10% ethyl acetate	>99	10.8	37.8	1.2	2	40.5	0	0	0	7.7	0	0	100
10% 1-propanol	>99	0	34.8	1.0	1.7	1.0	4.5	14.1	1.6	4.4	27.8	9.0	100
5% methanol	>99	0	100	0	0	0	0	0	0	0	0	0	100

Table 3. Effect of H₂ addition using 10 wt% acetic acid (balance H₂O) liquid feed over Zn₁Zr₁₀O₂ (T = 450°C, P_T = 1 atm, P_{N₂+H₂} = 0.50 atm, GHSV = 5,000 h⁻¹).

Feed (wt.%)	P _{total} (atm)	X _{carbon} (%)	Selectivity (mol C %)									Total
			CH ₄	CO ₂	Olefins				Alkanes	Acetone		
					C ₂	C ₃	C ₄	C ₅	C ₂ -C ₅			
10% acetic acid	0.5 N ₂	100	13.8	42.0	0.0	0.0	37.6	0.0	0.0	6.5	100.0	
10% acetic acid	0.4 N ₂ +0.1 H ₂	100	15.3	42.8	0.0	8.7	30.9	0.0	0.0	2.3	100.0	
10% acetic acid	0.25 N ₂ +0.25 H ₂	100	12.9	39.6	0.0	18.9	27.1	0.0	0.0	1.5	100.0	

Table 4. Effect of operating pressure when using 20 wt% ethanol (balance H₂O) liquid feed over Zn₁Zr₁₀O₂ (T = 450°C, P_T = 1 atm, P_{N₂} = 0.50 atm, GHSV = 5,000 h⁻¹).

Feed (wt.%)	P _{total} (atm)	X _{Carbon} (%)	Selectivity (mol C %)								Total
			CH ₄	CO ₂	Olefins			Alkanes	Acetone		
					C ₂	C ₃	C ₄	C ₅	C ₂ -C ₅		
20% Ethanol	1	100	6.8	32.3	1.8	5.5	42.5	0.0	0.0	11.1	100.0
20% Ethanol	7	100	5.3	32.1	1.1	6.8	36.1	0.7	0.0	17.9	100.0
20% Ethanol	20	100	7.7	34.3	1.3	10.9	37.6	0.0	0.1	8.1	100.0

Table 5. Effect of propanol addition to ethanol feed over Zn₁Zr₁₀O₂ (T = 450°C, P_T = 1 atm, P_{N₂} = 0.50 atm, GHSV = 5,000 h⁻¹).

Feed (wt.%)		T (°C)	X _{carbon} (%)	Selectivity (mol C %)												% Branched		
EtOH	PrOH			CH ₄	CO ₂	Olefins						Alkanes	Ketones		Total	C ₄	C ₅	C ₆
						C ₂	C ₃	C ₄	C ₅	C ₆	C ₂ -C ₅	Acetone	MEK	3-Pentanone				
10.0	10.0	450	100	2.0	20.6	0.6	1.1	6.1	21.3	10.3	0.3	10.9	25.1	1.5	100	76.3	>98	>98
15.0	5.0	450	100	3.3	24.5	0.8	2.1	16.1	22.2	9.2	0.2	18.3	2.9	0.3	100	92.0	>98	>98
17.5	2.5	450	100	3.9	24.8	0.8	2.9	23.2	14.6	8.4	0.1	19.8	1.4	0.1	100	96.4	>98	>98
20.0	0	450	100	6.8	32.2	1.7	5.4	42.4	0.0	0.0	0.0	11	0	0	100	100.0	N/A	N/A
15.0	5.0	375	90.7	0.0	17.3	1.0	0.6	0.6	0.2	0.0	0.0	42.1	37.5	0.7	100	17.0	100.0	>98
15.0	5.0	425	97.7	1.4	25.0	0.9	1.6	11.5	16.0	4.7	0.1	32.6	5.5	0.5	100	91.1	99.3	>98
15.0	5.0	450	100	3.3	24.5	0.8	2.1	16.1	22.2	9.2	0.2	18.3	2.9	0.3	100	92.0	98.9	>98

Table 6. Catalytic performance comparisons using a mixed oxygenate feed mixture (Table 1) over mixed oxide catalysts with varied acid and base properties (T = 450°C, P_T = 1 atm, P_{N₂} = 0.50 atm, GHSV = 3,800 h⁻¹).

Zr/Zn Ratio	X _{carbon} (%)	Selectivity (mol C %)									Total
		CH ₄	CO ₂	Olefins			Alkanes	Acetone			
				C ₂	C ₃	C ₄	C ₅	C ₂ -C ₅			
1/1	100	2.9	32.8	1.3	6.5	43.8	5.3	0.0	7.3	100	
2.5/1	100	3.6	33.7	1.2	6.9	46.9	2.8	0.0	4.9	100	
5/1	100	3.7	33.6	1.2	6.8	47.1	2.7	0.0	4.8	100	
10/1	100	2.8	34.8	1.7	6.2	44.5	3.3	0.0	6.6	100	
15/1	100	2.7	33.8	2.3	5.2	42.1	3.3	0.0	10.6	100	

Table 7. BET surface area, pore volume, pore diameter, acidity and basicity site quantification, and butene production as a function of Zr/Zn ratio.

Zr/Zn ratio	Surface area (m ² /g) ^a	Pore volume (cc/g) ^a	Pore diameter (nm)	Brönsted acid sites (μmoles/g) 150°C/ 350°C ^b	Lewis acid sites (μmoles/g) 150°C/ 350°C ^b	Basic sites ^c (μmoles/g)	Butene products ^d (sccm/g)
1/1	66.5	0.20	9.5	3.9/0	49.1/11.4	57.0	6.4
2.5/1	85.7	0.29	9.5	3.6/0	51.1/11.2	102.3	7.1
5/1	110.1	0.30	7.5	4.2/0	61.6/11.9	106.4	7.1
10/1	117.2	0.30	9.5	6.9/0.3	90.6/26.2	120.0	6.2

a. BET surface area, pore volume and pore diameter determined after N₂ adsorption.
b. b. From the IR spectra recorded after pyridine desorption at 150°C for 30 minutes (include weaker, medium and stronger acid sites) and after desorption at 350°C for 30 minutes (include only the stronger acid sites) From CO₂ chemisorption experiments.
c. Data extracted from Table 6.

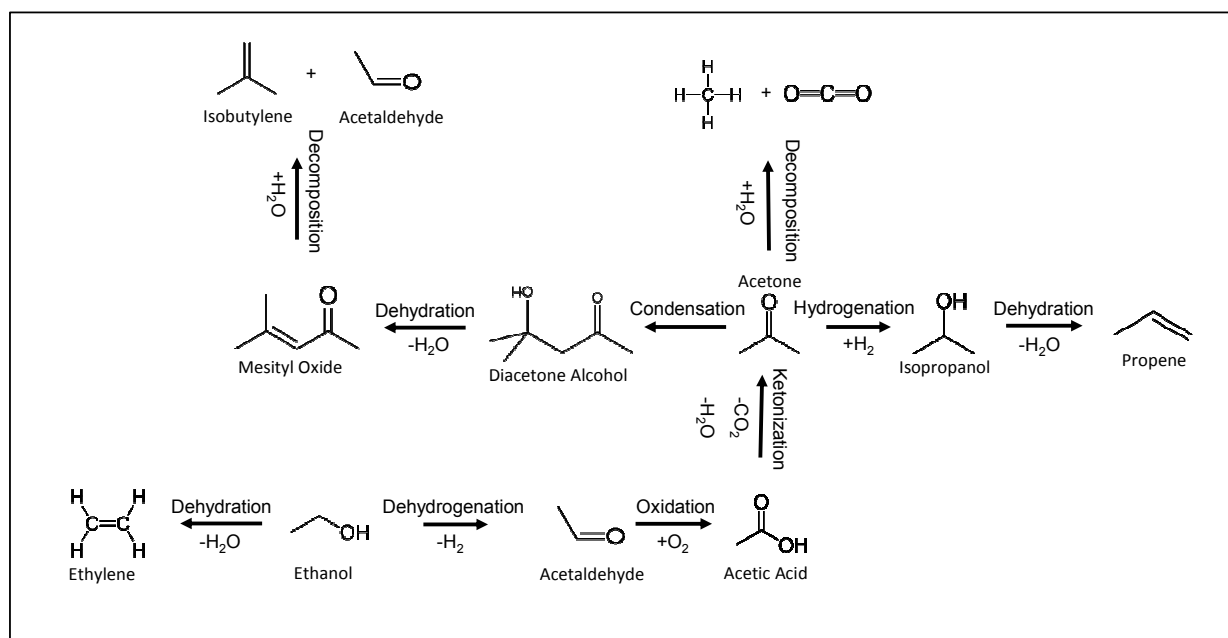


Figure 1. Reaction network for the conversion of ethanol to isobutene (and major side products).

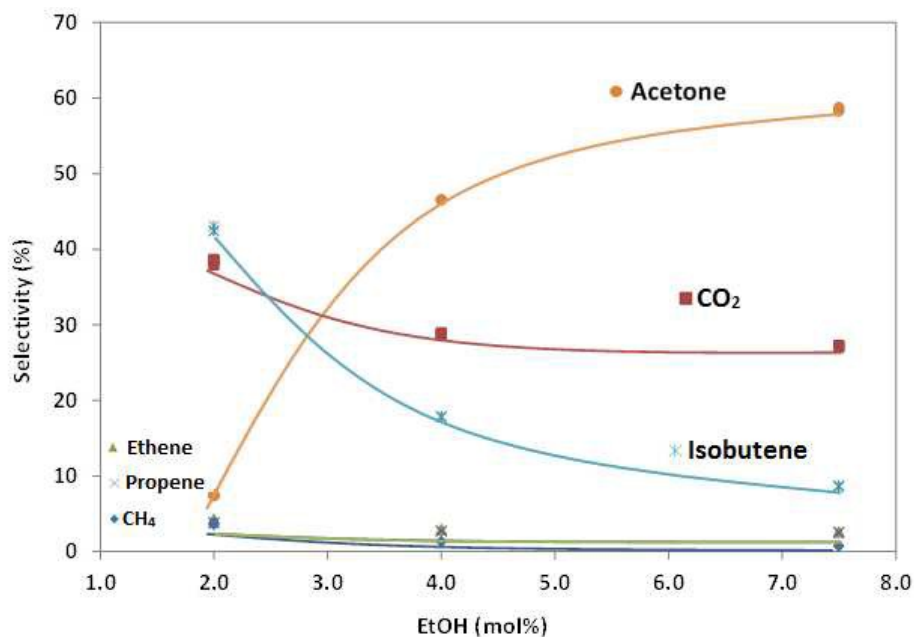


Figure 2. Effect of varying ethanol feed concentration on product selectivity over $\text{Zn}_1\text{Zr}_{10}\text{O}_2$ ($T = 425^\circ\text{C}$, $P = 1 \text{ atm}$, $\text{GHSV} = 15,500 \text{ h}^{-1}$, $\text{S/C} = 5 \text{ mol}$; ethanol conversion = 100% for all data points).

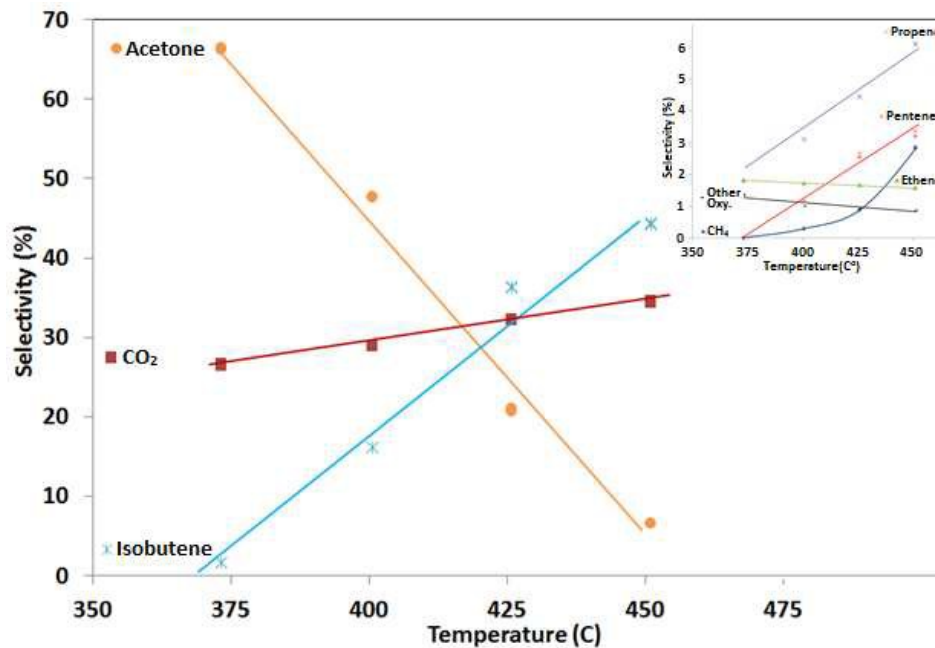


Figure 3. Effect of temperature on product selectivity for the mixed oxygenate feed mixture (Table 1) over Zn₁Zr₁₀O₂ ($P_T = 1$ atm, $P_{N_2} = 0.60$ atm, GHSV = 3,800 h⁻¹).

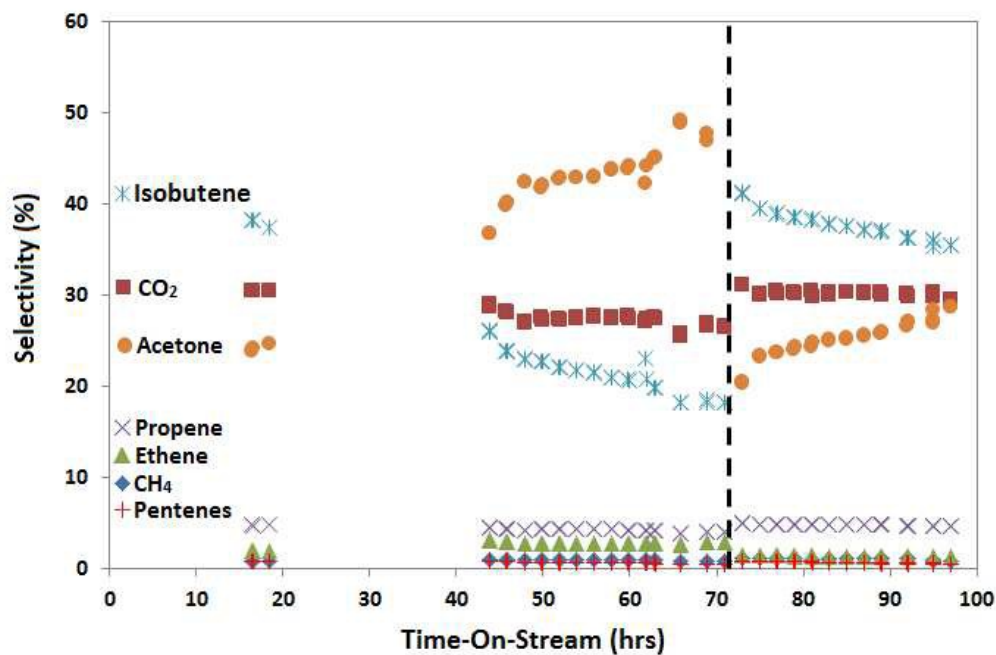


Figure 4. Stability and regeneration demonstration with the mixed oxygenate feed mixture (Table 1) over Zn₁Zr₁₀O₂. $T = 425^\circ\text{C}$, $P_T = 1$ atm, $P_{N_2} = 0.60$ atm, GHSV = 3,800 h⁻¹. Decoking

procedure performed via mild oxidative treatment after a time-on-stream of ~72 hours. Catalyst regeneration demonstrated as evidenced by selectivity recovery.

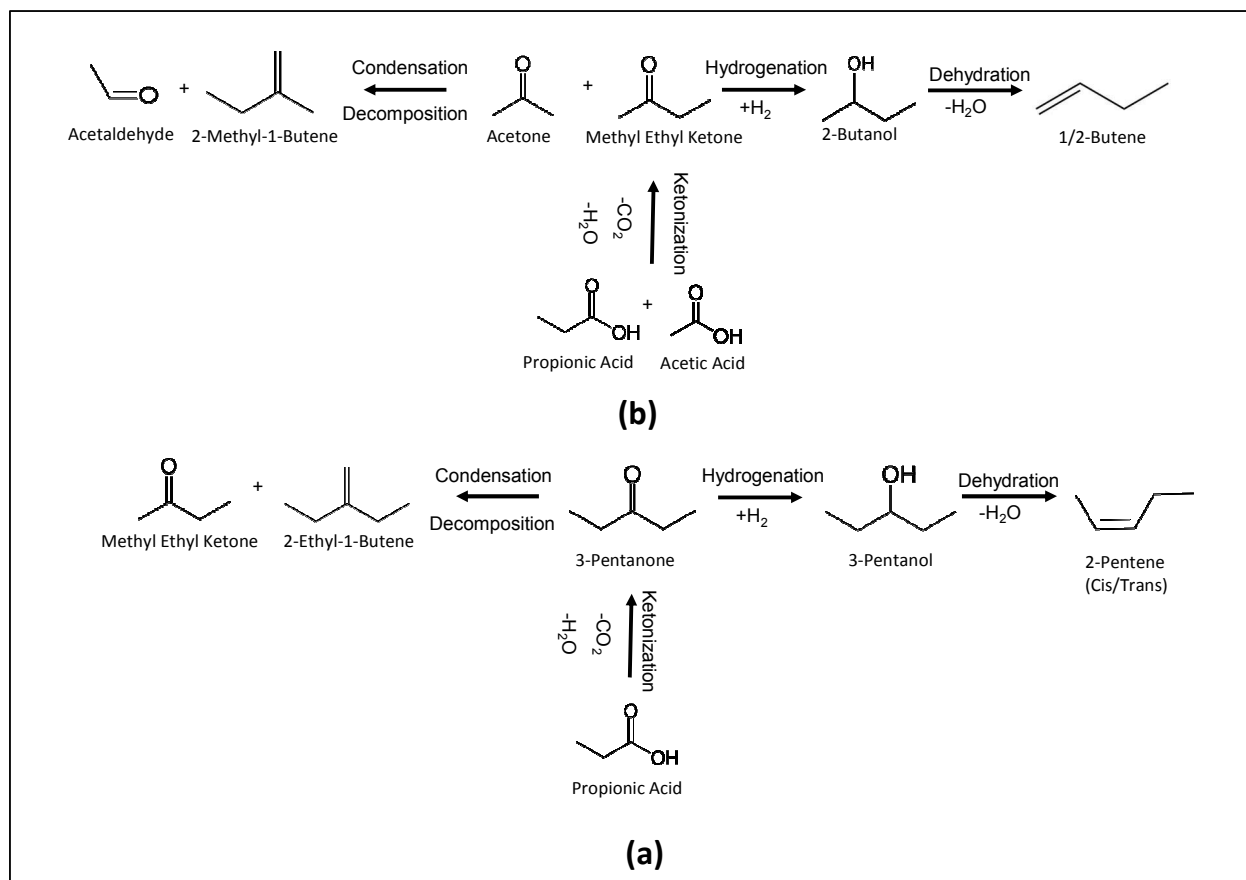


Figure 5. Reaction network for the conversion of (a) propanoic acid to form C₅ and C₆ olefins. Propanoic acid is formed from its parent alcohol propanol via dehydrogenation/oxidation as illustrated in Figure 1 and (b) propanoic acid and acetic acid mixtures to form C₄ and C₅ olefins. Propanoic and acetic acid are formed from their parent alcohol propanol and ethanol via dehydrogenation/oxidation as illustrated in Figure 1.

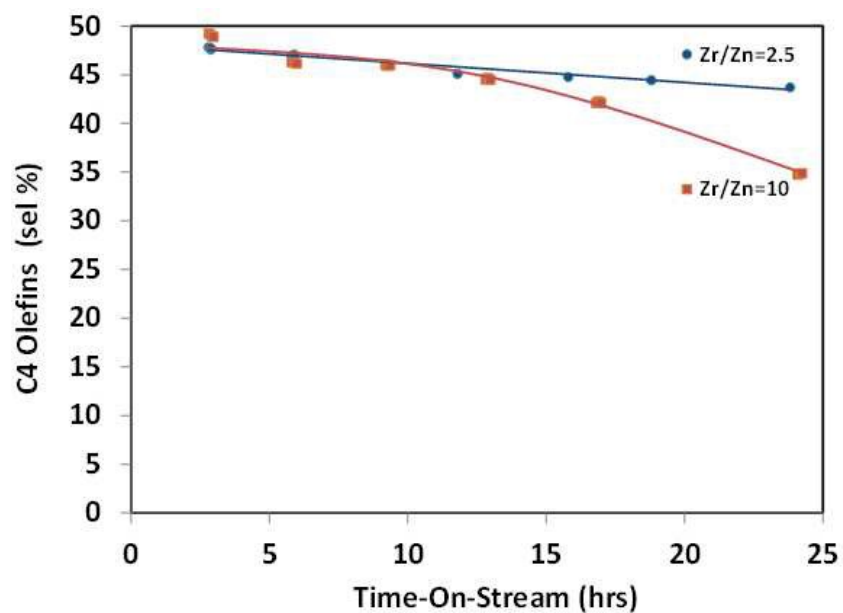


Figure 6. Stability comparison using the mixed oxygenate feed mixture (Table 1) over mixed oxide catalysts with varied acid and base properties. Catalysts: $Zn_1Zr_{10}O_2$ ($Zr/Zn = 10$) and $Zn_1Zr_{2.5}O_2$ ($Zr/Zn = 2.5$). $T = 425^\circ\text{C}$, $P_T = 1 \text{ atm}$, $P_{N_2} = 0.60 \text{ atm}$, $GHSV = 3,800 \text{ h}^{-1}$.

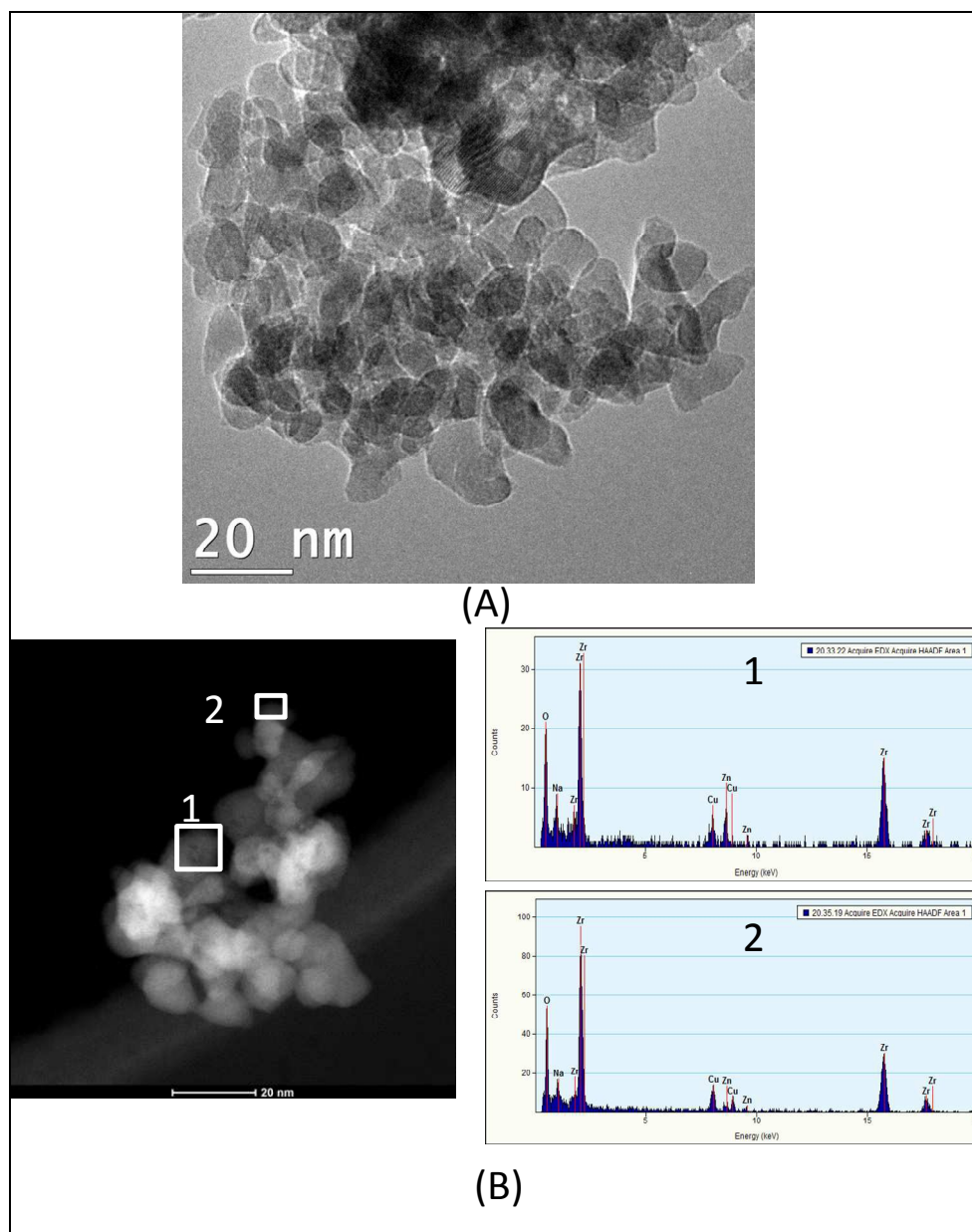


Figure 7. TEM (A) images and (B) EDX elemental mapping for the $\text{Zn}_1\text{Zr}_{2.5}\text{O}_2$ ($\text{Zr}/\text{Zn} = 2.5$) mixed oxide catalyst.

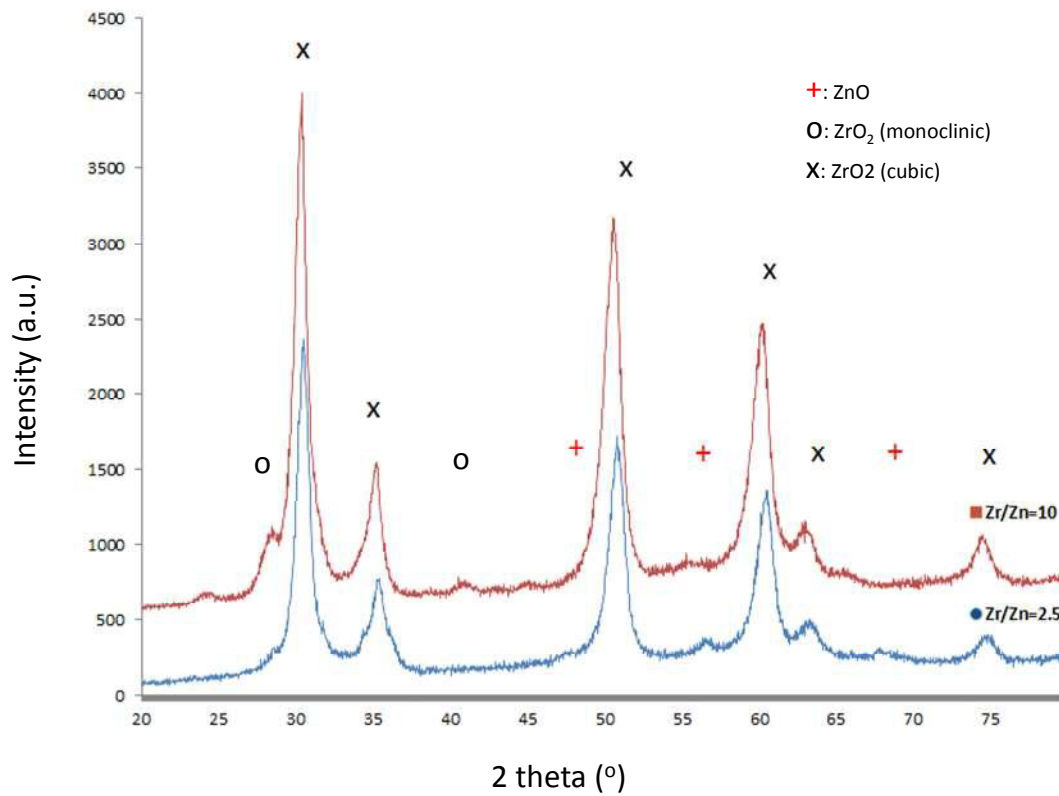


Figure 8. XRD patterns for the catalysts with Zr/Zn ratios equal to 2.5 and 10.

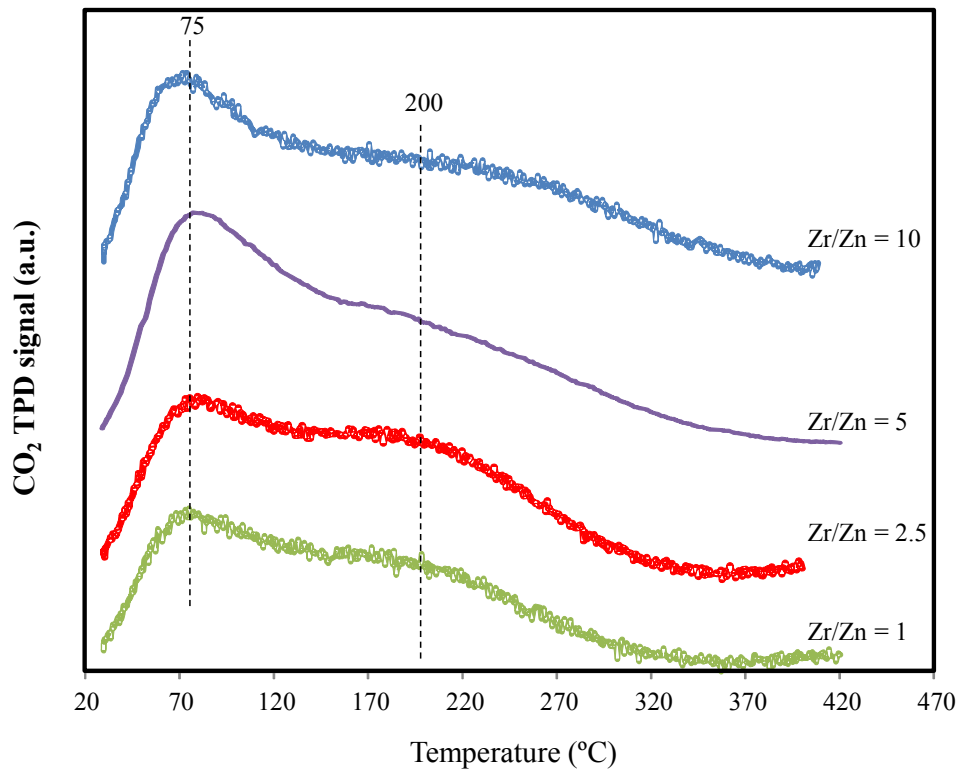


Figure 9. CO₂ TPD signal for the Zn_xZr_yO_z catalysts with Zr/Zn ratio between 1 and 10.

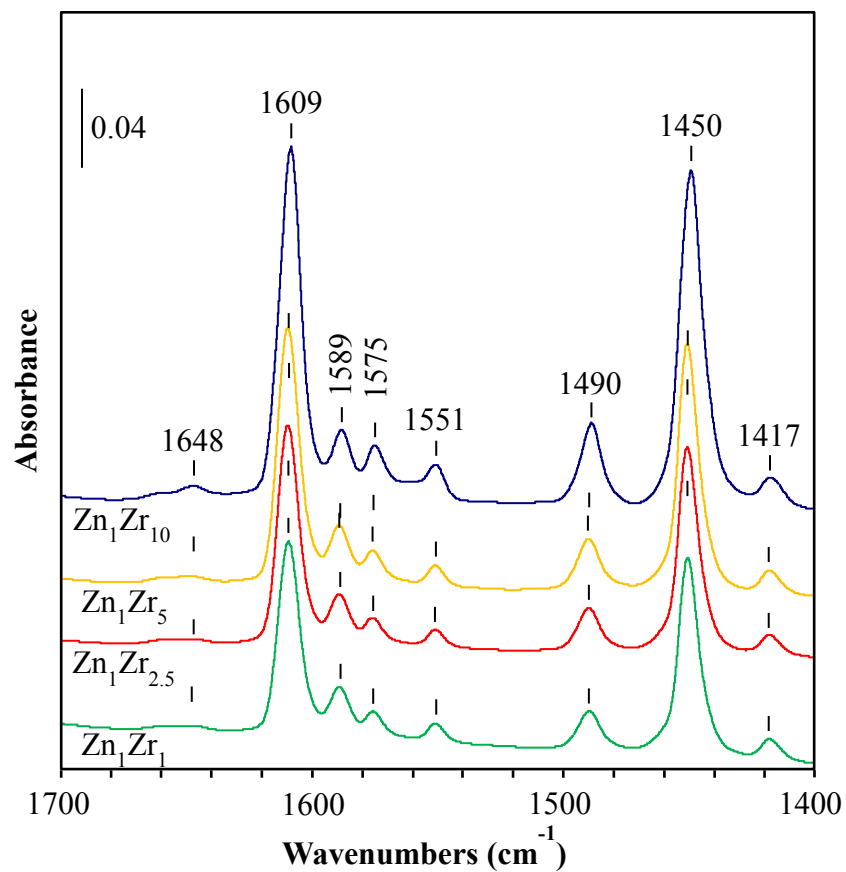


Figure 10. Infrared spectra recorded after pyridine adsorption at 150°C followed by desorption at the same temperature for 30 minutes. Spectra normalized to 10 mg of catalyst and for a pellet of 2 cm².

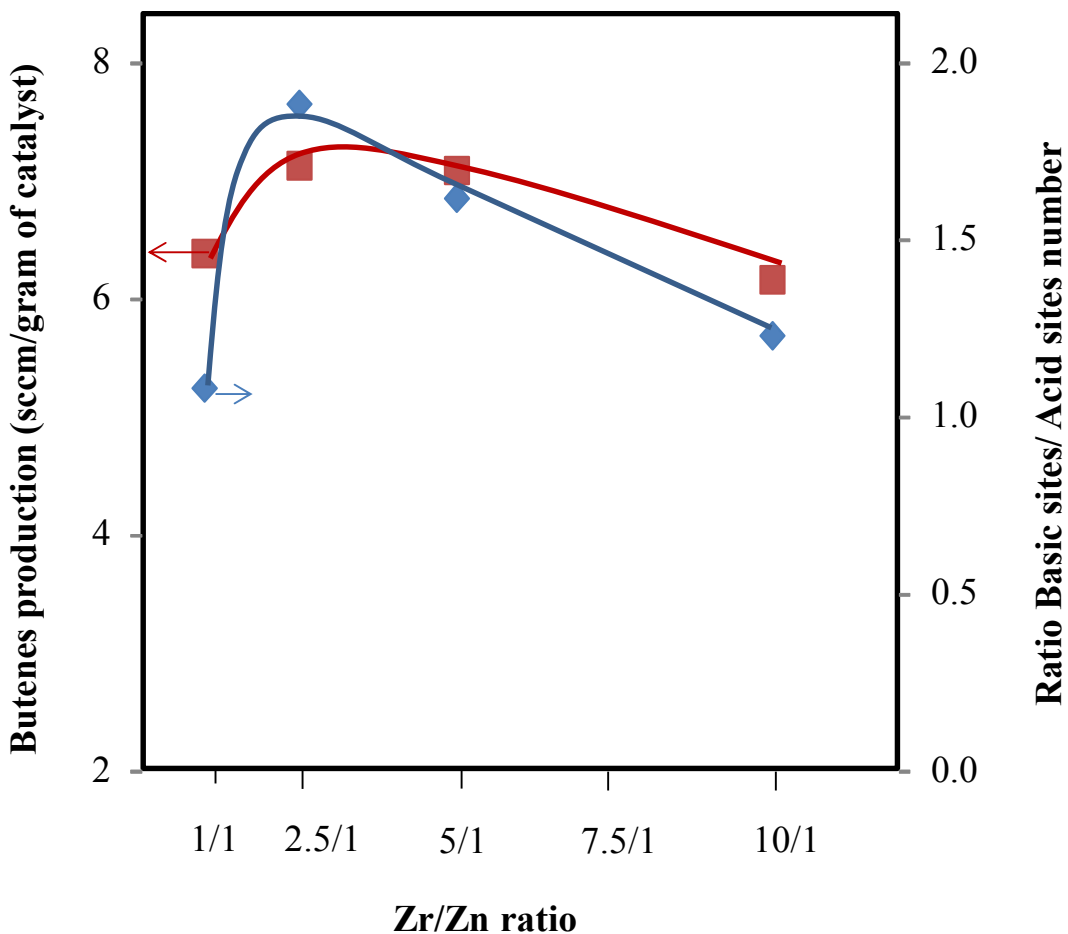


Figure 11. Relationship between butene production (activity data extracted from Table 6) and the ratio of basic to acidic sites as a function of the Zr/Zn ratio. The acid sites concentration was determined from the IR spectra collected after pyridine desorption at 150°C.

References

1. J. N. Chheda and J. A. Dumesic, *Catal. Today*, 2007, **123**, 59.
2. J. Goldemberg, *Science*, 2007, **315**, 808.
3. G. W. Huber, S. Iborra and A. Corma, *Chem. Rev.*, 2006, **106**, 4044.
4. A. Corma, S. Iborra and A. Velty, *Chem. Rev.*, 2007, **107**, 2411-2502.
5. J. N. Chheda, G. W. Huber and J. A. Dumesic, *Angew. Chem.-Int. Edit.*, 2007, **46**, 7164-7183.
6. J. Sun and Y. Wang, *ACS Catalysis*, 2014, **4**, 1078-1090.
7. G. W. Huber, S. Iborra and A. Corma, *Chem. Rev.*, 2006, **106**, 4044-4098.
8. G. Chen, C.-Y. Guo, X. Zhang, Z. Huang and G. Yuan, *Fuel Processing Technology*, 2011, **92**, 456-461.
9. J. J. Spivey and A. Egbebi, *Chemical Society Reviews*, 2007, **36**, 1514-1528.
10. E. Panisko, T. Wietsma, T. Lemmon, K. Albrecht and D. Howe, *Biomass and Bioenergy*, 2015, **74**, 162-171.
11. G. A. Deluga, J. R. Salge, L. D. Schmidt and X. E. Verykios, *Science*, 2004, **303**, 993.
12. R. S. Murthy, P. Patnaik, P. Sidheswaran and M. Jayamani, *J. Catal.*, 1988, **109**, 298.
13. T. Tago, H. Konno, S. Ikeda, S. Yamazaki, W. Ninomiya, Y. Nakasaka and T. Masuda, *Catalysis Today*, 2011, **164**, 158-162.
14. J. Sun, K. Zhu, F. Gao, C. Wang, J. Liu, C. H. F. Peden and Y. Wang, *Journal of the American Chemical Society*, 2011, **133**, 11096-11099.
15. C. Liu, J. Sun, C. Smith and Y. Wang, *Applied Catalysis A: General*, 2013, **467**, 91-97.
16. *USA Pat.*, 2014.
17. J. Q. Bond, D. M. Alonso, D. Wang, R. M. West and J. A. Dumesic, *Science*, 2010, **327**, 1110-1114.
18. J. W. Yoon, J. S. Chang, H. D. Lee, T. J. Kim and S. H. Jung, *J. Catal.*, 2007, **245**, 253.
19. C. Butler and C. P. Nicolaides, *Catal. Today*, 1993, **18**, 443.
20. V. M. Lebarbier, A. M. Karim, M. H. Engelhard, Y. Wu, B.-Q. Xu, E. J. Petersen, A. K. Datye and Y. Wang, *ChemSusChem*, 2011, **4**, 1679-1684.
21. D. Bish and S. Howard, *J Appl. Cryst.*, 1988, **21**, 86-91.
22. C. A. Emeis, *Journal of Catalysis*, 1993, **141**, 347-354.
23. L. Kubelková, J. Čjka, J. Nováková, V. Boszácek, I. Jirka and P. Jíaru, in *Studies in Surface Science and Catalysis*, eds. P. A. Jacobs and R. A. v. Santen, Elsevier, 1989, vol. Volume 49, pp. 1203-1212.
24. T. Nakajima, K. Tanabe, T. Yamaguchi, I. Matsuzaki and S. Mishima, *Applied Catalysis*, 1989, **52**, 237-248.
25. M. I. Zaki, M. A. Hasan and L. Pasupulety, *Langmuir*, 2001, **17**, 768-774.
26. A. I. Biaglow, J. Sepa, R. J. Gorte and D. White, *Journal of Catalysis*, 1995, **151**, 373-384.
27. A. G. Panov and J. J. Fripiat, *Journal of Catalysis*, 1998, **178**, 188-197.
28. M. A. Hasan, M. I. Zaki and L. Pasupulety, *Applied Catalysis A: General*, 2003, **243**, 81-92.
29. L. K. Freidlin and V. Z. Sharf, *Russ Chem Bull*, 1958, **7**, 1220-1226.
30. S. Thotla, V. Agarwal and S. M. Mahajani, *Chemical Engineering Science*, 2007, **62**, 5567-5574.

31. M.A. Gerber, M.J. Gray, K.O. Albrecht, B.L. Thompson, *Optimization of Rhodium-Based Catalysts for Mixed Alcohol Synthesis – 2012 Progress Report*, Pacific Northwest National Laboratory Report, 2012, PNNL-22659.
32. M.A Gerber, M.J. Gray, B.L. Thompson, *Long-Term Testing of Rhodium-Based Catalysts for Mixed Alcohol Synthesis*, Pacific Northwest National Laboratory Report, 2013, PNNL-22786.
33. V. A. Glezakou, J. E. Jaffe, R. Rousseau, D. H. Mei, S. M. Kathmann, K. O. Albrecht, M. J. Gray and M. A. Gerber, *Topics in Catalysis*, 2012, **55**, 595-600.
34. D. Mei, R. Rousseau, S. M. Kathmann, V.-A. Glezakou, M. H. Engelhard, W. Jiang, C. Wang, M. A. Gerber, J. F. White and D. J. Stevens, *Journal of Catalysis*, 2010, **271**, 325-342.
35. A. B. Trenwith, *Journal of the Chemical Society (Resumed)*, 1963, DOI: 10.1039/JR9630004426, 4426-4430.
36. A. Feinberg and C. H. Perry, *Journal of Physics and Chemistry of Solids*, 1981, **42**, 513-518.
37. T. Hirata, E. Asari and M. Kitajima, *Journal of Solid State Chemistry*, 1994, **110**, 201-207.
38. J. C. Lavalley, J. Saussey and C. Bovet, *Journal of Molecular Structure*, 1982, **80**, 191-194.
39. T. Onfroy, G. Clet, S. Bukallah, D. Hercules and M. Houalla, *Catalysis Letters*, 2003, **89**, 15-19.